Heat Flow and Arc Efficiency at High Pressures in Argon and Helium Tungsten Arcs

Experiments are conducted with the GTAW process in a pressurized dry chamber to simulate underwater welding

BY A. KATSAOUNIS

ABSTRACT. For control of welding underwater robotic systems, the arc characteristics and the heat quotation in cathode, arc column and anode (weld) were measured in GTAW with argon and helium shielding gas using the calorimetric method. The measurements were performed mainly in a pressure chamber. The pressure, the current and the arc length were varied from 0.1–6.0 MPa, 50–300 A and 2–11 mm, respectively. It was observed that the welding voltage is strongly dependent on system pressure for both shielding gases and an explicit minimum voltage/current was obtained for the argon arc characteristics at approximately 100 A. Furthermore, the field strength and the heat emission from the arc column increased exponentially with the pressure. A simple relation was developed to predict heat emission from the arc column and, consequently, for the arc efficiency. In addition, a calculation model for engineering use was derived based on the Ellenbaas-Heller equation to calculate the-heat flux from the arc to the weld (for both gases).

Introduction

Welding is a necessary and important process for repair and maintenance of underwater installations. Despite this fact, not enough detailed information is available for the GTAW arc as the welding heat source in dry, high-pressure, underwater environments.

GTAW arcs have long been used as heat sources for welding under normal ambient conditions. For underwater tasks, welding is usually done in a dry, high-pressure — equivalent to water depth — environment. More information is needed about the heat loss from the arc column to the surroundings to predict arc efficiency; *i.e.*, the heat flux to the weld, considering the influence of the most relevant parameters in welding. The heat flux initiates the welding process and together with some other factors — such as the heat transfer from the weld to the surroundings (weld cooling), weld formation, and alloy content — is relevant for the weld quality.

Experimental results will be presented for GTAW simulated conditions performed with argon and helium shielding gas in a pressure chamber. The arc characteristics and the heat quotation in the cathode, arc column and anode (weld) were measured using the calorimetric method. The pressure, the current and the length of the arc were varied for argon in the range from 0.1–6.0 MPa, 50–300 A and 2–11 mm, respectively. Furthermore, some relevant parameters such as the shielding gas flow rate, the vertex angle of the electrode conical tip, the composition of the cathode (tungsten with ThO_2, LaO_2, ZrO_2), and the alloy in the weld pool were varied in order to study their influence on the heat transfer to the anode.

Additionally, for predicting the effective arc radius, a calculation model for engineering use was derived based on the Ellenbaas-Heller equation (one dimensional heat conduction equation with homogeneously distributed heat sources and sinks). The effective arc radius is needed for the calculation of the heat flux on the weld as a function of pressure, current and arc length.

KEY WORDS

Heat Flow
Arc Efficiency
GTAW
Modeling
Argon Shielding Gas
Helium Shielding Gas
Ellenbaas-Heller Eq.
1-D Model

Description of the Test Facility

All measurements were performed by the GKSS-Research Center in a simple test facility consisting mainly of calorimeters installed in a dry pressure chamber working in a pressure range of 0.1–10 MPa. Additionally a small pump circulated water from these calorimeters to a heat exchanger, and a valve at the front of each calorimeter regulated the inlet cooling water mass flow.

A commercial size welding rectifier with descending operating characteristics was used for arc burning (Ref. 1). The arc was ignited by short circuit. After arc ignition, the welding torch (cathode) was moved upwards by an apparatus. The length of the arc; *i.e.*, the distance between anode and cathode, was measured twice: at the beginning and at the end of each measurement. The latter measured value was assumed to be the actual arc length. For all experiments, the tungsten electrode had a diameter of 3.2 mm.

The anode and the arc column calorimeters are shown in Fig. 1. The anode — a 200-mm diameter by 20-mm thick smooth steel plate — was arranged on a smooth copper plate equipped at the upper side with 13 NiCr-Ni thermocouples for measurement of the radial temperature distribution below the steel plate. The surfaces of the steel plate were covered with insulating material. The upper insulation plate was equipped with 8 NiCr-Ni thermocouples for measurement of the upper side temperature distribution — Fig. 1. The inlet and the

A. KATSAOUNIS is Professor für Thermische Verfahrenstechnik at TFH-Berlin, Berlin, Germany.

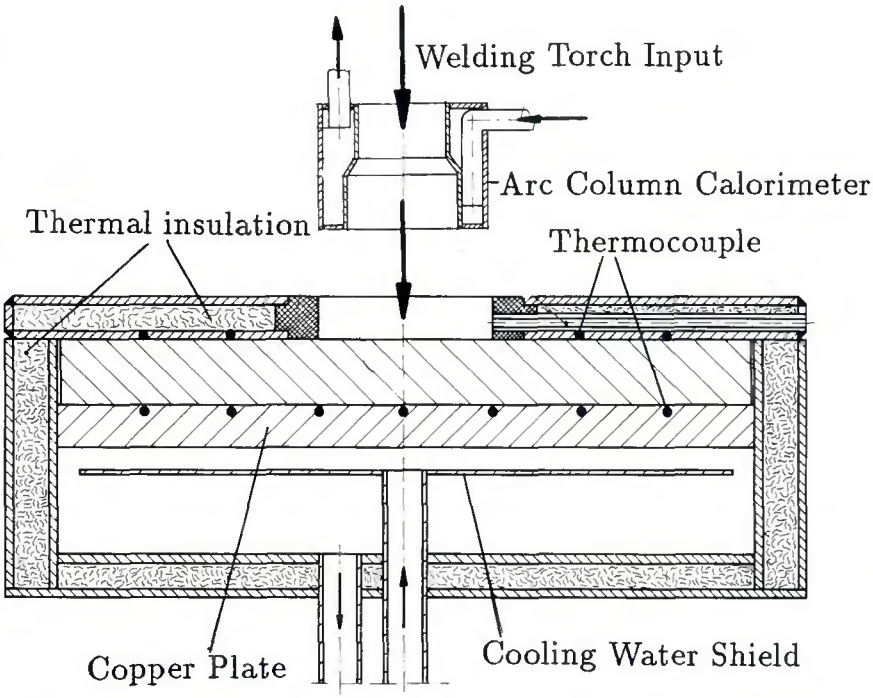

Fig. 1 — The design of the calorimeters.

outlet of cooling water were located at the calorimeter bottom (Ref. 1).

The arc column calorimeter is the most sensitive component of the test facility because of its design — Fig. 1. The copper calorimeter walls are only 1 mm thick. The heat emission from the arc column, which rises considerably with increasing current, arc length and pressure, produces a very strong thermal load inside of the calorimeter walls. The wall outside was covered by thin fiberglass insulation tape.

The gas mass flow rate and the temperatures at the inlet and outlet of the welding torch calorimeter were measured by a turbine flowmeter and NiCr-Ni thermocouples to control the heat input to the shielding gas, needed for heat balance (Ref. 1). The welding torch cooling system was assembled and used as a calorimeter for measuring the power input necessary to heat the tungsten electrode (cathode). Thus the NiCr-Ni thermocouples used to measure the inlet and outlet water temperatures were placed very close to the collet of the electrode to make sure that only the heat supplied to the tungsten electrode was measured (Ref. 1).

The maximum statistical errors of the measured heat fluxes for anode, arc column and torch calorimeter were calculated with ±12.2%, ±2.1% and ±1.4%, respectively. The prediction was made considering the measuring range, the individual error of the installed devices and the VDI/VDE German standards for error propagation (Ref. 1).

The thermocouples on the upper side of the copper plate in the anode calorimeter were used to detect the thermal equilibrium. If no temperature change was measured, thermal equilibrium was achieved and data recording was started. Data recording began approximately 33–60 s after arc ignition (Ref. 1).

A detailed description of the test facility design, measuring techniques, a list of all measured data and the computer code used are given in Ref. 1.

Arc Characteristics

Considering the stability criterion of Kaufmann (Ref. 2), an arc burns stable if the voltage drop increases with the current; *i.e.*

$$\frac{dU}{dI} > 0 \qquad (1)$$

This criterion was used to qualify the welding process considering the arc characteristics.

Arc Characteristics at Atmospheric Pressure

The influence of 1) gas flow rate between 5–15 standard L^3 of gas per minute (dm_n^3/min); 2) the vertex angle of the electrode conical tip varied between 20–90 deg for argon, and between 20–60 deg for helium; 3) the cathode composition (tungsten with 1% ThO_2, or 1% LaO_2, or 0.8% ZrO_2); and 4) the weld pool alloy (STE 445.7 and STE 415 with the compositions in %: C 0.16, Si 0.41, Mn 1.6, P 0.015, S 0.004, N 0.013, Al 0.015, Ni 0.36, V 0.016, remainder Fe, and C 0.14, Si 0.27, Mn 1.4, P 0.019, S 0.003, Al 0.031, rest Fe respectively) on the arc characteristic were investigated at atmospheric pressure in argon and helium shielding gas in addition to the main parameters, current and arc length.

Of all the above mentioned parameters, only the vertex angle of the conical tip had a significant influence on the welding voltage in argon shielding gas (Ref. 1). The welding voltage for 90 deg was approximately one volt less compared with the data for 45 and 20 deg for all measured arc lengths. The results of the measurements performed with 45 and 20 deg vertex angle of conical tip did not differ relative to voltage deviation. These results are similar to those obtained by Savage, *et al.* (Ref. 3), Chichoski (Ref. 4) and Petric-Pfender (Ref. 5). The rise in the voltage with increasing vortex angle can be explained if one considers that during welding the cathode spot of the arc moves upward along the flank of the conical tip to the islands of higher oxide (ThO_2) concentration. The movement of the cathode spot upward effects an increase in arc length and thus the welding voltage rises.

The measurements in helium were performed using electrodes with 20, 45 and 60 deg vertex angle conical tips. For these conditions, no significant influence of the vertex angle of the conical tip on the welding voltage drop was measured for helium shielding gas.

The arc characteristics for argon shielding gas are plotted — Fig. 2. The minimum of all curves is achieved at $I_{min} \approx 85$ A. For helium shielding gas, the minimum is observed at $I_{min} \approx 200$ A (Ref. 1). Considering the stability criterion of Kaufmann, Equation 1, an unstable arc behavior was expected for all currents less than I_{min}, while for higher currents the voltage drop rose with increasing welding current and the arc burned stably.

For argon shielding gas and currents higher than 85 A (dU/dI > 0), the measurements are compatible with those of Allum (Ref. 6) — Fig. 3. Similar results (Ref. 1) were obtained from a comparison between our data and measurements and those of Dijk-den Ouden (Ref. 7) and Savage, *et al.* (Ref. 3).

In a diagram of welding voltage vs. arc length with the current as parameter, the fitting curves through the measured points $U = f(l_b, I)$ were extrapolated for $lim(l_b) \rightarrow 0$ to cut the ordinate axis (Ref. 1). This voltage drop on the axis corresponds to the sum of the anode and cathode fall voltage $(U_{a,c} = U_a + U_c)$ immediately after the start of arc burning. The average electric field strength

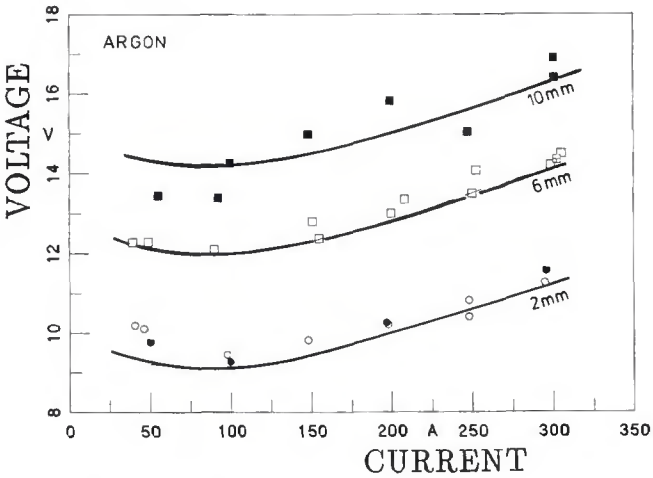

Fig. 2 — Voltage-current arc characteristics for argon at atmospheric pressure. Tungsten electrode 1% ThO_2, 45 deg vertex angle of conical tip, 10 dm_n^3/min gas flow.

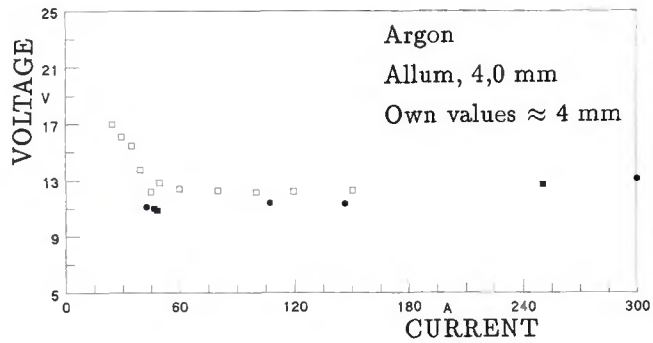

Fig. 3 — Voltage-current arc characteristics at atmospheric pressure in parameter range. A — Allum (Ref. 6): no gas flow, 60 deg vertex angle of conical tip; B — present work: 10 dm_n^3/min gas flow, 45 deg vertex angle of conical tip.

of the arc column is defined by the equation

$$E = \frac{U - (U_a + U_c)}{l_b} \quad (2)$$

Considering Equation 2, an empirical relation is developed from the experimental data to predict the arc column field strength at atmospheric pressure for argon

$$E_{0.1} = 0.881 - 0.22 \cdot (l_b / 10) \quad (3)$$

and for helium shielding gas

$$E_{0.1} = 2.15 - 0.6 \cdot (l_b / 10) \quad (4)$$

respectively — Fig. 4. The integration of both equations over the arc length boundaries l_{max} = 11 mm and l_{min} = 2 mm gives an average electric arc field strength of $E_{0.1}$ = 0.75 V/mm for all measured arc lengths in argon, which corresponds to the value predicted by Allum (Ref. 6). The corresponding average field strength value for helium shielding gas is $E_{0.1}$ = 1.88 V/mm.

Arc Characteristics at High Pressures

All measurements at high pressures between 0.5 and 6.0 MPa in argon shielding gas were performed for 2, 6 and 10 mm arc lengths. In helium only experiments at pressures up to 2.0 MPa and for 2 and 6 mm arc lengths with a current of 100 A were conducted.

Increasing pressure and current shortens the life and increases the abrasion of the electrode. This effect is more pronounced for measurements in helium shielding gas. At high pressures and currents, the commercial size orifice for the shielding gas has been replaced by an orifice constructed from high-temperature melting material.

Experimental data for voltage drop vs. arc length in argon shielding gas were plotted at a current of 100 A — Fig. 5. The U = f(l_b,I) lines were extrapolated to cut the ordinate axis for $lim(l_b) \rightarrow 0$ in order to estimate the sum of anode and cathode voltage drop $U_{a,c}$, needed for the prediction of the electric arc field strength according to Equation 2.

The voltage vs. current diagram in Fig. 5 shows arc characteristics typical for arcs in the region of $6 \leq l_b \leq 7$ mm, which are strongly dependent on pressure. This figure also shows that for argon shielding gas an explicit minimum in the voltage-current arc characteristics occurs at approximately 100 A. This minimum is more distinct at higher pressures. Arc instabilities were observed at high pressures for currents less than 70 A. These are probably related to the form of the arc characteristics. Compare Equation 1.

In addition, the measured values were plotted in a voltage drop vs. pressure diagram (Ref. 1). Figure 6 shows sam-

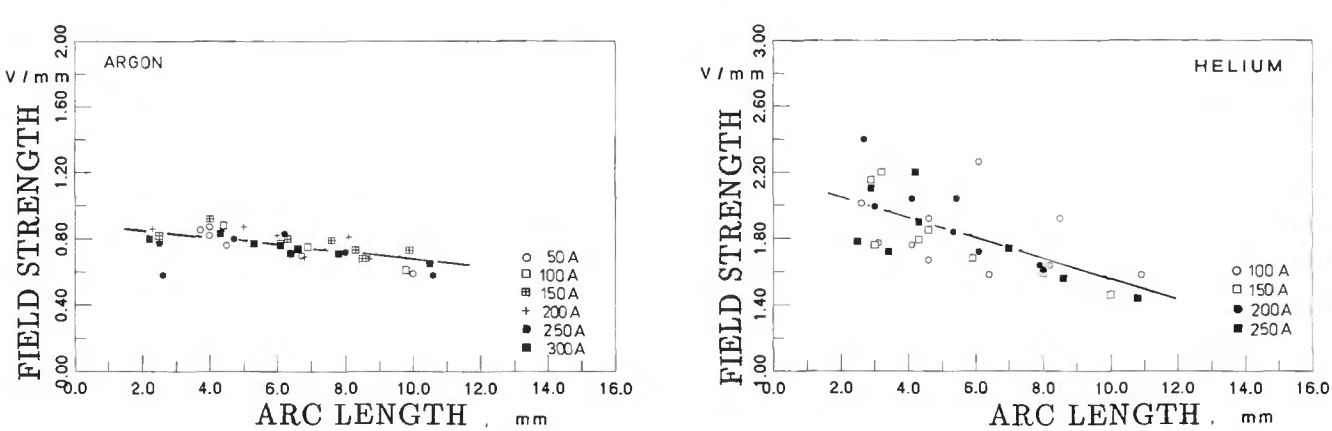

Fig. 4 — Electric arc field strength vs. arc length at atmospheric pressure. Comparison of Equation 3 with argon data (left) and Equation 4 with helium data (right).

ples taken at 100 A and at different arc lengths. The Allum (Ref. 6) data in the same figure agree with our measurements. Both sets of measurements were made for a comparable parameter region.

The marks at the plotted points in Figs. 5 through 7 relate to the actual measured arc lengths. The fitting curves through the measured data in Figs. 5 and 6 were drawn to be consistent in all these figures.

The data obtained in helium shielding gas are shown in Fig. 7 and the data corresponding to those for argon are shown in Figs. 5 and 6. A selection of measured data obtained by Allum (Ref. 6) and Dijkden Ouden (Ref. 7) for a comparable parameter region has been plotted into the diagrams. Acceptable agreement between all experimental data can be obtained from these diagrams.

With Equation 2 and Fig. 5, the arc field strengths were calculated as a function of the pressure. Considering the alternating effect between the arc column, electron potential and kinetic energy (Ref. 1) the equation

$$E = E_{0.1} \cdot \left(\frac{p}{p_{0.1}}\right)^n \tag{5}$$

is derived, where $E_{o.i}$ is the arc field strength at atmospheric pressure predicted from Equation 3. The exponent n has been correlated with all experimental data to be equal to 0.4 (n = 0.4) for all arc lengths and currents in argon shielding gas.

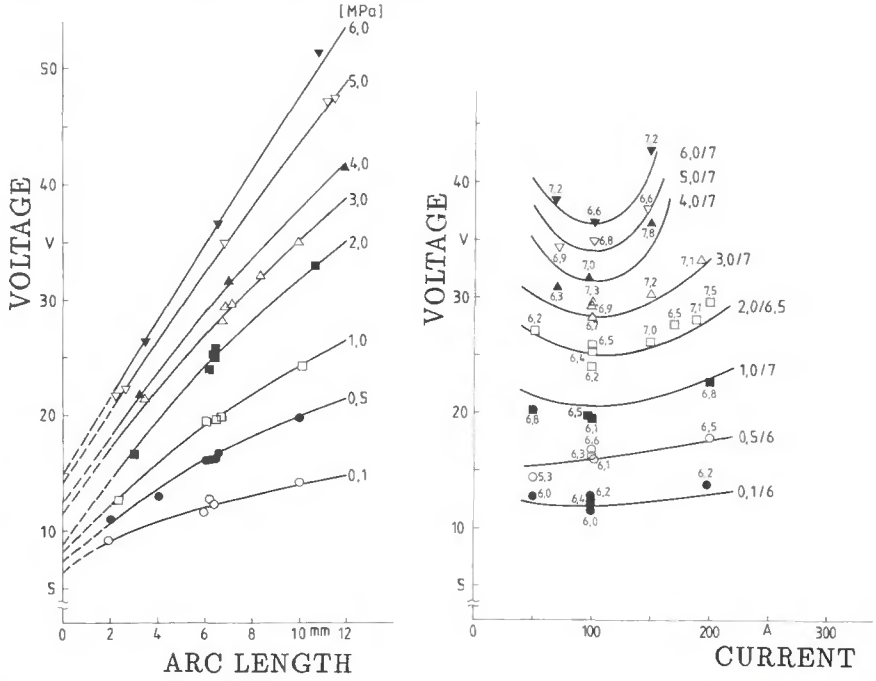

Fig. 5 — Voltage-arc-length arc characteristics for a current of 100 A and voltage-current arc characteristics for 7 mm arc length.

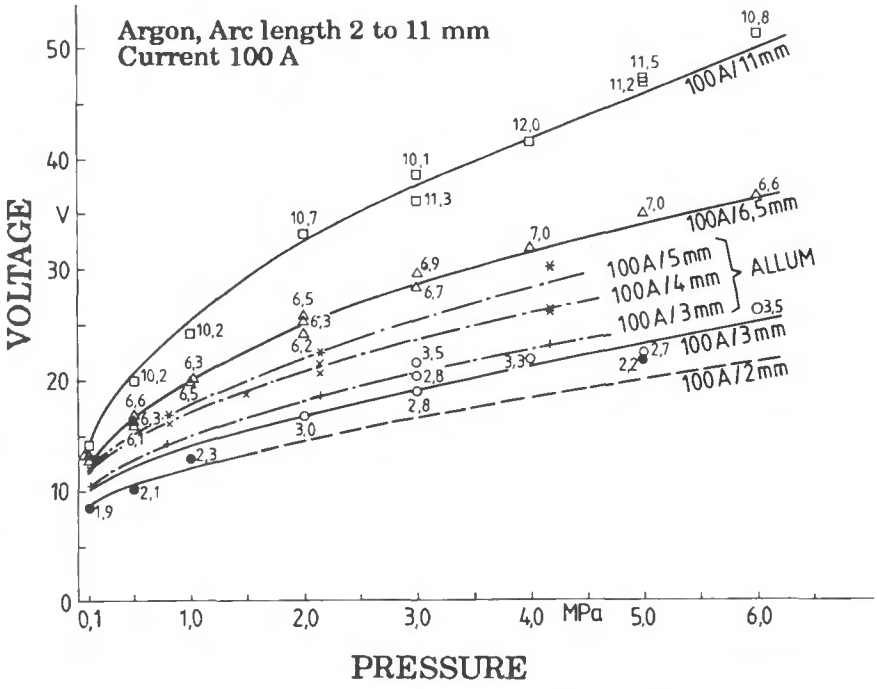

Fig. 6 — Arc characteristics for voltage drop vs. pressure with a current of 100 A in argon.

Arc Efficiency

The energy efficiency-factors defined as arc efficiency

$$\eta_W = \frac{\dot{Q}_W}{U \cdot I} \tag{6}$$

radiation loss factor

$$\eta_l = \frac{\dot{Q}_{lb}}{U \cdot I} \tag{7}$$

and cathode energy loss factor

$$\eta_e = \frac{\dot{Q}_e}{U \cdot I} \tag{8}$$

are plotted vs. total input power $(U \cdot I)$ as shown in Fig. 8 for argon (left) and helium (right) shielding gas at atmospheric pressure. All experiments were performed using a tungsten electrode with 1% ThO_2 by a 45 deg vertex angle conical tip (WT1O/45 deg) and a gas flow rate of 10 dm_n^3/min for both shielding gases.

Finally, applying the balance equation if the shielding gas heating energy is negligible gives

$$\eta_W + \eta_l + \eta_e = \eta_g = 1 \tag{9}$$

The cathode energy factor can be predicted for instance in argon shielding gas by the equation $\eta_e = 0.084 - 0.012Q$ (Ref. 1) — Fig. 8. The cathode energy loss factors was calculated approximately by

$$\eta_e = 0.08 \text{ for argon} \quad \text{and}$$
$$\eta_e = 0.04 \text{ for helium} \tag{10}$$

shielding gas. The cathode energy loss factor is pressure independent and for argon it is twice as high as for helium

shielding gas (Ref. 1). It can be seen from Fig. 8 that the cathode energy loss factor is smaller compared with all other efficiency factors.

Assuming equal current and arc length for both gases, the voltage drop in argon is appreciably less than in helium shielding gas. Thus for identical conditions, the total input power for helium is considerably higher than for argon. For all measurements in argon and helium shielding gas, the same tungsten electrode was used; consequently, the same input energy was needed for both gases for electrode heating and for electron extraction from the cathode. The higher cathode energy loss factor for argon shielding gas can be also explained with respect to Equation 8, because $(U \cdot I)$ for helium is higher than for argon.

Following a line of constant current or arc length in Fig. 8, the radial loss factor η_l for both shielding gases increases with increasing total input power; therefore, the arc efficiency decreases as the radiation heat is increasing. This is reasonable if one considers that with increasing current and arc length, both the mean temperature (Refs. 9 through 11) and the radiation source strength S in the arc column are rising.

Referring to the above remarks, for equivalent arc burning conditions in both shielding gases, the voltage drop in helium is considerably higher (about 50%) than in argon shielding gas, and thus the total input power must be higher for helium. Figure 8 shows an equal current line (i.e., 100 A) for argon and helium shielding gas. Approximately the same arc efficiency value can be read in both gases, if nearly 50% higher total input power is considered for helium, corresponding to the higher helium voltage at equivalent conditions.

Although the pressure affects the voltage drop in helium more strongly than in argon shielding gas (compare Figs. 6 and 7), the radiation loss factor and the arc efficiency show similar dependencies on the pressure. From Fig. 9 it can be seen that the deviation between the efficiencies in both shielding gases is not higher than 5%.

Prediction of the Heat Flux to the Weld

For the prediction of heat conduction events in the weld region; *i.e.*, molten metal zone and heat-affected zone (HAZ), the heat flux to the weld

$$\dot{q}_W = \frac{\dot{Q}_W}{A} \tag{11}$$

has to be determined. For the calculation of the heat flux, either the weld heat flow $\dot{Q}_W$ or the arc efficiency η_W, and the effective radius R of the arc column for predicting the heat input area $A = \pi R^2$ must be known.

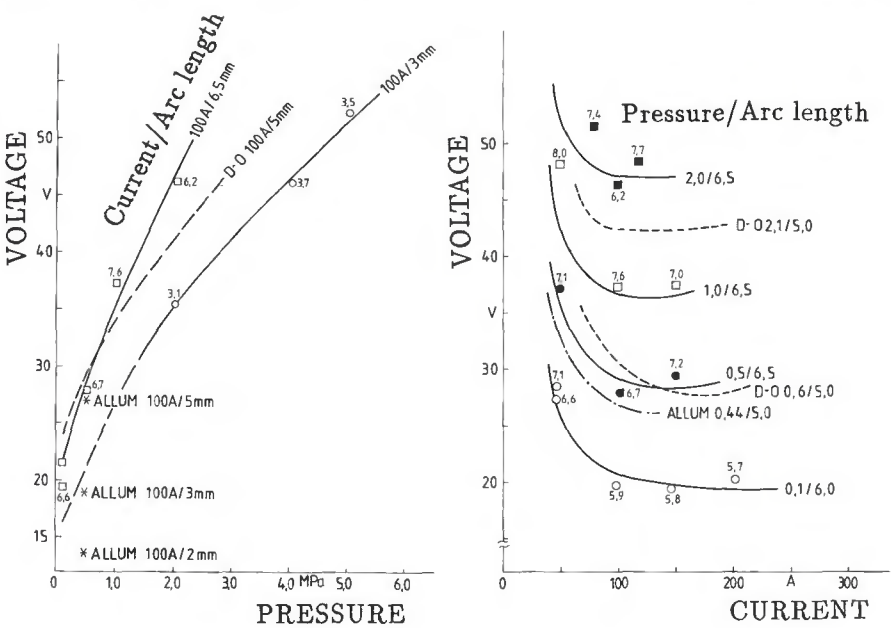

Fig. 7 — Voltage-pressure (left) and voltage-current (right) arc characteristics for helium.

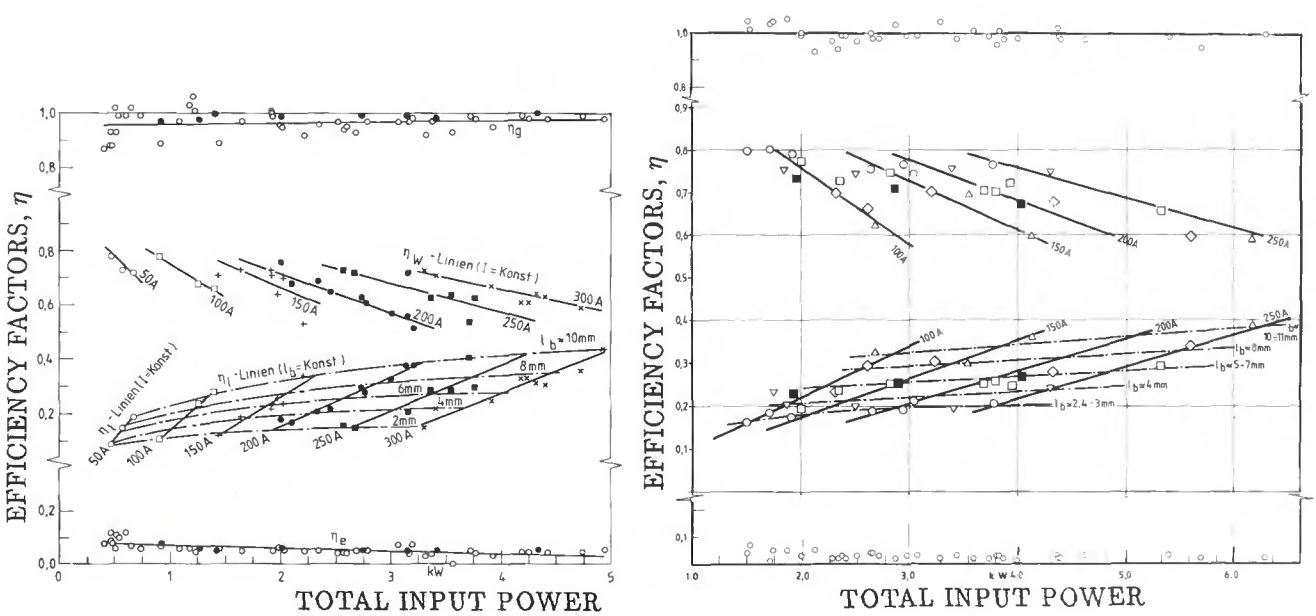

Fig. 8 — Efficiency factors η vs. total input power at atmospheric pressure for argon (left) and helium (right) shielding gas.

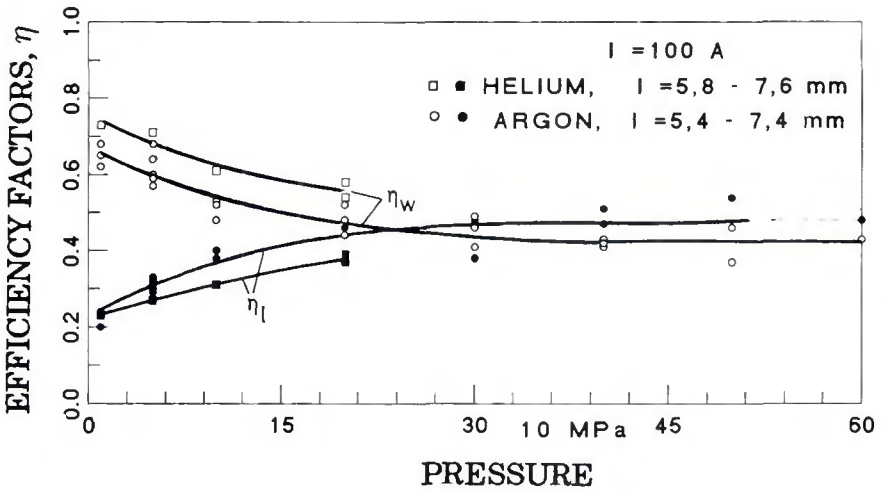

Fig. 9 — Radiation loss factor and arc efficiency for argon and helium vs. pressure.

Calculation of the Arc Radiation Quotient

Heat emission Q_{lb} from the arc column to the surroundings in relation to the power supplied in the arc column ($\pi R^2 l_b \sigma E^2$), called arc radiation quotient κ, is defined (Ref. 1) by the equation

$$\kappa = \frac{\dot{Q}_{lb}}{\pi R^2 l_b \sigma E^2} \qquad (12)$$

where σ (S/m) is the electrical conductivity of the arc plasma.

All properties are referred to the mean arc column plasma temperature given by the equation

$$\overline{T} = \frac{2}{R^2}\int_0^R Trdr \qquad (13)$$

Using the above assumption, the current intensity

$$I = 2\pi E\int_0^R \sigma rdr \qquad (14)$$

can be integrated and Equation 12 will be changed to

$$\kappa = \frac{\dot{Q}_{lb}}{EIl_b} \qquad (15)$$

Considering Equation 5, the above equation can be further rearranged into the form

$$\kappa = \frac{\dot{Q}_{lb}}{E_{0.1} Il_b (p/p_{0.1})^n} \qquad (16)$$

From the correlation of Equations 15 and 16 with all the experimental data obtained in argon and helium shielding gas, the exponent n is found to be equal 0.48 (n = 0.48) for both gases. The arc radiation quotient κ is in the range of $50 \le I \le 300$ A for argon

$$\kappa_{argon} = 0.292 + 0.23\left(\frac{I}{100}\right) \qquad (17)$$

and in the range $100 \le I \le 250$ A for helium shielding gas

$$\kappa_{helium} = 0.43 \pm 0.04 \qquad (18)$$

Finally, using Equations 3 and 17 for argon and Equations 4 and 18 for helium, the radiation heat flow from the arc column can be derived as

$$\dot{Q}_{lb} = \kappa E_{0.1} Il_b \left(\frac{p}{p_{0.1}}\right)^{0.48} \qquad (19)$$

Consequently, with Equation 7, the radiation loss factor η_l, Equations 9 and 10, the arc efficiency η_w, and Equation 6, the input heat flow to the weld, Q_w can be predicted.

Calculation of the Effective Arc Column Radius

Considering the Ellenbaas-Heller energy equation — a one-dimensional[1] steady-state heat conduction equation including distributed heat sources in the arc plasma — the arc input power per unit volume and unit time is σE^2. The heat losses from the control volume element per unit time by conduction is $-\frac{1}{r}\frac{d}{dr}\left(\lambda r \frac{dT}{dr}\right)$ and by radiation the source strength is S(r,T). Consequently, the well known differential equation

$$(\sigma \cdot E^2 - S) + \frac{1}{r}\cdot\frac{d}{dr}\cdot\left(\lambda \cdot r \cdot \frac{dT}{dr}\right) = 0 \qquad (20)$$

is valid. For the prediction of the effective radius and temperature distribution in the arc column, Equations 14 and 20 must be solved simultaneously. So the following assumptions must be made:

1) The arc column is for a sufficient distance from both ends (anode and cathode). A cylindrical continuum including the heat sources and σE^2 is homogeneously distributed over the total volume $\pi R^2 l_b$ of the arc column.

2) Since experimental measurements show that the heat portion transferred from the arc column into the shielding gas is approximately 0.5% of the total input power, it can be assumed that the heat losses from the arc column occur mainly by radiation to the surroundings and less by convection and conduction at the interface area (r = R) between gas flow and arc column plasma.

3) Furthermore, it is assumed that the plasma behaves like a gray body so that the Stefan-Boltzmann equation is valid:

$$E_s(T, p) = \varepsilon(T, p) C_s T^4 \qquad (21)$$

where $\varepsilon(T,p) \le 1$ is the emission coefficient and $C_s = 5.77\ 10^{-8}\ W/m^2K^4$ the Stefan-Boltzmann constant.

The heat conductivity $\lambda(T, p)$, electrical conductivity $\sigma(T, p)$ and radiation source strength $S(T, p)$ (Refs. 8 and 13 through 16) are functions of temperature and pressure.

Usually Equations 14 and 20 can be solved numerically. An analytical solution of both equations for engineering use is available if one assumes that the arc column temperature profile within the range $0 \le r \le R$ is so flat that a function of the form

$$\overline{f(\overline{T})} = \frac{2}{R^2}\cdot\int_0^R f(T)\cdot r\cdot dr \qquad (22)$$

can be accepted for the calculation of the mean value for the plasma properties. In contrast to the above assumption, it must be assumed in this case that the total heat radiation is originating from an area $2\pi r_s 2l_b$, so that the equation

$$S(\overline{T})\cdot\pi\cdot R^2\cdot l_b = 2\pi\cdot r_s\cdot l_b\cdot E_s(\overline{T}) \qquad (23)$$

1 *The use of a one-dimensional equation to predict the heat flux from the arc to the weld is a low cost method, requiring relatively short computational time. It is designed for engineering use only. Comparison between experimental data and the one-dimensional calculations has shown these calculations to be acceptable for engineering use.*

Anyone working in heat and/or hydrodynamics is familiar with three-dimensional solutions to equation systems, which produce results if the physical phenomena are well known. In all other cases, assumptions must be made in considering unknown physical processes. Wherever assumptions must be made, involved calculations become only of academic interest and are not very successful for engineering or practical use because of the uncertainty introduced by the assumptions, despite the long time periods invested in computation.

is valid, where r_s, $(r_s \leq R)$ is the radius of the heat emission area, and T_s is the corresponding heat radiation temperature. Finally, the emission coefficient ε can be calculated from the equation

$$\varepsilon = \frac{S \cdot R^2}{2 \cdot r_s \cdot C_s \cdot T_s^4} \leq 1 \qquad (24)$$

According to the above assumptions, Equation 14 is integrated to

$$I = \pi \sigma E R^2 \qquad (25)$$

and Equation 20 is rearranged into the form

$$\frac{d^2T}{dr^2} + \frac{1}{r} \cdot \frac{dT}{dr} + \frac{\sigma \cdot E^2}{\lambda} = 0 \qquad (26)$$

Considering the boundary conditions

$$\lambda \cdot \frac{dT}{dr}\Big|_{r=0} = 0 \quad \text{and}$$
$$T = T_R \quad \text{for} \quad r = R \qquad (27)$$

the solution for Equation 26 found in Ref. 16 is

$$T = T_R + \frac{E \cdot I}{4\pi \cdot \lambda} \cdot \left[1 - \left(\frac{r}{R}\right)^2\right] \qquad (28)$$

If the ordinate r_s is known, the arc column temperature gradient and the effective arc column radius R can be predicted from the above equations. One of the possible assumptions for r_s is that the mean radiation temperature T_s is equal to the mean arc column temperature $\bar{T}$. Consequently the ordinate r_s is equal to the radius $r_{\bar{T}}$, *i.e.*, $r_s = \sqrt{\bar{T}}$. The mean temperature of the arc column

$$\bar{T} = T_R + \frac{1}{8\pi} \cdot \frac{E \cdot I}{\lambda} \qquad (29)$$

was calculated from Equations 13, 25 and 28. Furthermore, considering Equations 17, 18, 19, 21 and 13, the temperature gradient in the arc column can be calculated from the equation

$$T = \left[\left(\frac{\sqrt{2} \cdot \kappa}{2\pi}\right) \cdot \frac{E_{0,1} \cdot I}{R \cdot C_s \cdot \varepsilon} \cdot \left(\frac{p}{p_1}\right)^{0,48}\right]^{1/4} + \frac{E \cdot I}{4\pi \cdot \lambda} \cdot \left(\frac{1}{2} - \left(\frac{r}{R}\right)^2\right) \qquad (30)$$

Finally, the mean radiation temperature is predicted by the equation

$$\bar{T} = \left[\left(\frac{\sqrt{2} \cdot \kappa}{2\pi}\right) \cdot \frac{E_{0,1} \cdot I}{R \cdot C_s \cdot \varepsilon} \cdot \left(\frac{p}{p_1}\right)^{0,48}\right]^{1/4} \qquad (31)$$

while the corresponding radius is

$$r_{\bar{T}} = R / \sqrt{2} \qquad (32)$$

Measured arc column radii obtained by Allum (Ref. 6) for a current of 100 A and for a 3.2-mm arc length were plotted vs. pressure — Fig. 10. In the same figure, the calculated arc column radii for a 6-mm arc length, predicted using the model derived above, are shown for comparison. The agreement between measured and experimental values is acceptable.

Conclusions

In argon shielding gas, the welding voltage drop decreases with increasing vertex angle of the electrode conical tip. For vertex angles less than 45 deg, no significant influence of the vertex angle on the voltage drop was found.

Welding voltage is strongly dependent on system pressure in both shielding gases. In helium shielding gas, the arc voltage increases with higher pressure than in argon. This behavior results in a higher thermal load for the electrode (cathode) and for the shielding gas nozzle in helium.

For argon shielding gas an explicit minimum in voltage-current arc characteristics was obtained at approximately 100 A. This minimum is more distinct at higher pressures. For currents less than 70 A at high pressures, arc instabilities were observed, probably caused by the form of the arc characteristics.

Electric field strength of the arc column — a necessary input for the calculation of the arc efficiency — depends insignificantly on the arc length at atmospheric pressure. The field strength increases exponentially with the pressure, due to the physical behavior of the arc plasma at higher pressures.

Arc efficiency η_w at atmospheric pressure for argon and helium shielding gas decreases with increasing total input power in the same manner as the radiation loss factor increases along a constant line for current or arc length.

The radiation loss factors have approximately the same slope for both shielding gases up to 3.0 MPa pressure. At pressures higher than 3.0 MPa, no significant change of the radiation loss factor with the pressure was observed in argon shielding gas. Therefore, arc efficiency decreases as the radiation loss factor increases with the pressure.

The radiated heat from the arc column increases exponentially with pressure. The exponent is the same for both shielding gases. A simple equation was developed to predict the heat emission from the arc column to the environment and consequently for the prediction of the arc efficiency.

Furthermore, for engineering use a calculation model was derived based on the Ellenbaas-Heller differential equation to predict the effective arc radius and, consequently, the heat flux from the arc to the weld as a function of pressure, current and arc length. If the heat flux is known, the volume and dimensions of the weld, as well as the heat conduction behavior in the surroundings of the weld (HAZ) can be calculated using a suitable computer code.

Appendix

Nomenclature

A area, *m*
C_s Stefan-Boltzmann Constant, $Wm^{-2}K^{-4}$
E field strength, V_{nm-1} or Vm^{-1}
E_s emission of black body, Wm^{-2}
I current, *A*
lb Arc Length, mm
n exponent
p pressure, *MPa*

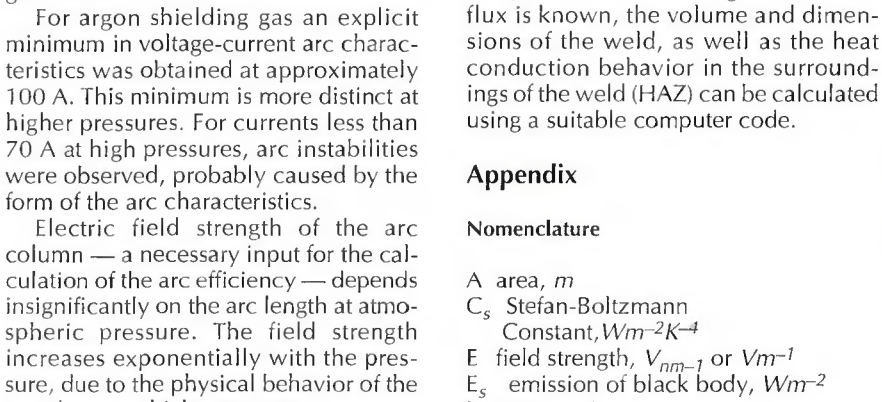

Fig. 10 — Arc column radius vs. pressure as predicted and measured by Allum (Ref. 6).

Q heat flow, W
q heat flux, Wm^{-2}
R,r radius, m
S radiation source strength, Wm^{-3}
T temperature, K
T mean temperature of arc column, K
U voltage drop, V
ε emission coefficient
η efficiency factor
κ arc radiation quotient
λ heat conductivity, $Wm^{-1}\ K^{-1}$
σ Electrical Conductivity, Sm^{-1}, $\Omega^{-1}\ m^{-1}$

References

1. Katsaounis, A. 1990. *Untersuchungen zum Lichtbogenwirkungsgrad beim WIG-SchweiBen fuer Druecke bis 6.0 MPa.*, Public Report GKSS 90/E/6, GKSS-Research Center Geesthacht, F.R. Germany

2. Finkelnburg, W., and Maecker, H. 1956. *Elektrische Boegen und thermisches Plasma. Handbuch der Physik. Band XXII Gasentladungen II.* Eds. Fluegge, H., Berlin, Springer Verlag.

3. Savage, W. F., Strunck, S. S. and Iscikawa, Y. 1965. The effect of electrode geometry in gas tungsten arc welding. *Welding Journal* 486-s to 496-s.

4. Chichoski, R. A. 1970. The rationing of power between the gas tungsten arc and electrode. *Welding Journal* 69-s to 82-s.

5. Petric, T. W., and Pfender, E. 1970. The influence of the cathode tip on temperature and velocity fields in a gas-tungsten arc. *Welding Journal* 588-s to 596-s.

6. Allum, C. J. 1982. The characteristics and structures of high pressure (1–42 bars) gas tungsten arcs I und II. Ph. D. Thesis, Cranfield Institute of Technology, School of Industrial Science.

7. Dijk, O., and den Ouden, G. 1983. The effect of pressure on the TIC- welding process. *Proc. of the Intern. Underwater-Welding Conference*, Trondheim/Norway.

8. Bauder, U. W. 1976. Properties of high pressure arc plasma. *Appl. Physics. 9*:105 to 115.

9. Milner, D. R., Salter, G. R. and Wilkinson, J. B. 1960. Arc characteristics and their significance in welding. *Brit. Welding J.*: 73 to 88.

10. Haddad, G. N., and Farmer, A. J. D. 1985. Temperature measurements in gas tungsten arcs. *Welding Journal* 339-s to 342-s.

11. Tsao, K. C., and Pavelic, V. 1979. Spectroscopic studies of a constricted argon plasma arc. *Proc. Int. Conf. Arc Physics and Weld Pool Behaviour*, London/UK.

12. Emmons, H. W. 1967. Arc measurements of high-temperature gas transport properties. *Phys. Fluids. 10*: 112S to 36.

13. Devoto, R. S. 1971. Transport coefficients of high pressure argon in a magnetic field. Aerosp. Res. Lab. ARL 71-0075.

14. Devoto, R. S. 1973. Transport coefficients of ionized argon. *Phys. Fluids. 16*: 616 to 23.

15 Vargaftik, N. B. 1975. *Tables on the Thermophysical Properties of Liquids and Gases.* Second Edition. Hemisphere Publishing Corp. Washington, London.

16. Grigull, U. 1963. *Die Grundlagen der Wärmeuebertragung.* Berlin, Springer Verlag.